Aquacultural Engineering 90 (2020) 102086

Contents lists available at ScienceDirect

Aquacultural Engineering

journal homepage: www.elsevier.com/locate/aque

Hydrodynamic characteristics of a full-scale kelp model for aquaculture applications

David W. Fredriksson[a,*], Tobias Dewhurst[b], Andrew Drach[c], William Beaver[d], Adam T. St. Gelais[e,f], Kathryn Johndrow[e], Barry A. Costa-Pierce[e,f]

[a] Department of Naval Architecture and Ocean Engineering, United States Naval Academy, 590 Holloway Road, 11D Annapolis, MD 21402 USA
[b] Kelson Marine Co., Scarborough, Maine 04074 USA
[c] University of Texas at Austin. Austin, Texas 78712 USA
[d] Hydromechanics Laboratory, United States Naval Academy, 590 Holloway Road, 11D Annapolis, MD 21402 USA
[e] Graduate Program in Ocean Food Systems, School of Marine & Environmental Programs, University of New England, 11 Hills Beach Road, Biddeford, Maine 04005 USA
[f] School of Marine and Environmental Programs, University of New England, 11 Hills Beach Road, Biddeford, Maine 04005 USA

ARTICLE INFO

Keywords:
Macroalgae hydrodynamics
Aquaculture physical model
Reconfiguration of kelp
Saccharina latissima

ABSTRACT

Hydrodynamic characteristics are needed to optimize the design of kelp aquaculture systems. To support this need, the objective of this study was to resolve both the normal and tangential drag forces acting on a dense aggregate of kelp blades using full-scale physical model tests. The physical model was designed to match the exposed length, individual blade flexural rigidity, the number of blades per unit width, the mass/length of biomass, and the aggregate mass density of kelp cultured at the University of New England experimental aquaculture lease site in Saco Bay, Maine USA. Tow tests were conducted at the United States Naval Academy in a tank with the dimensions of 116m × 7.9m × 4.9 m. The large tank size enabled the use of the full-scale physical model, minimizing dynamic similarity issues. In a series of tests, the model was towed in orientations both aligned and perpendicular to the tow direction. Horizontal and vertical reaction forces were measured for five tow speeds, along with the deflection of the dense kelp aggregate. With these datasets and the wet weight biomass per length of the model, normal and tangential drag forces were calculated. Drag components were processed into corresponding normal and tangential drag-area values. The drag-area representation was chosen since reference areas were ambiguous for both the actual kelp and model. At the higher speeds, the total horizontal drag in the aligned configuration were slightly lower than for the perpendicular orientation. Normal drag-areas as a function of tow speed ranged from 2.36 m^2/m to 1.39 m^2/m for the aligned case and from 2.49 to 1.88 m^2/m for the perpendicular case. Tangential drag-areas as a function of tow speed ranged from 0.264 m^2/m to 0.0325 m^2/m for the aligned case and from 0.213 to 0.0415 m^2/m for the perpendicular case. A transition from a bluff body to a streamlined body occurred as the tow speeds increased. To investigate this transition, horizontal components of the normal and tangential drag forces were reconstructed with the results of the tow tests. The reconstructed forces were obtained using a force balance system of equations with drag-area values for tow speeds less than 0.25 m/s extrapolated from the experimental datasets. For both aligned and perpendicular orientations, the model-aggregate reconfigured at a threshold of 0.25 m/s. We defined the threshold for reconfiguration as the tow speed at which the horizontal component of tangential drag equaled or exceeded the horizontal component of the normal drag. The drag-area results from this study can be incorporated into a dynamic fluid-structure interaction model representing kelp aggregates as a finite element beam prescribed with *in-situ* values of length, volume, mass density and flexural-rigidity of kelp material.

1. Introduction

The development of a large scale macroalgae aquaculture industry will depend upon maximizing yield per cost. Maximizing yield implies high yield (e.g. > 20 kg/m) if *Laminariales* (kelp) systems employ either individual or arrays of kelp lines/structures. Optimization of such systems provides an engineering challenge to characterize and quantify the hydrodynamic behavior of a unique material, in this case, densely

* Corresponding author.
E-mail addresses: fredriks@usna.edu (D.W. Fredriksson), Toby@KelsonMarine.com (T. Dewhurst), andrew.drach@utexas.edu (A. Drach), wmbeaver@usna.edu (W. Beaver), astgelais@une.edu (A.T. St. Gelais), kjohndrow@une.edu (K. Johndrow), bcostapierce@une.edu (B.A. Costa-Pierce).

https://doi.org/10.1016/j.aquaeng.2020.102086
Received 16 November 2019; Received in revised form 4 April 2020; Accepted 5 April 2020
Available online 04 May 2020
0144-8609/

seeded and compliant kelp. Single blade reconfigurations of flexible algae (Gaylord and Denny, 1997; Boller and Carrington, 2006; Luhar and Nepf, 2017) have been shown to reduce the frontal area making it more streamlined. Buck and Buchholz (2005) examined the drag characteristics of both single and clumps of blades (13 blades per clump) of *Saccharina latissima* (sugar kelp), examining the hydrodynamic responses of kelp with drag force expressed as a function of the tow velocity squared, adjusted with a "figure of merit" term described by Vogel (1984). Buck and Buchholz (2005) showed that the angle of the blades changed with increasing current velocities, becoming nearly horizontal at high speeds. Another important observation was a reduction of drag values per blade in the aggregated, 13 blade configuration. Thus, the hydrodynamic behavior of aggregated kelp cannot be estimated by superimposing the behavior of individual blades. The work of Vettori and Nikora (2019) was similar to that of Buck and Buchholz (2005) using single blades of *S. latissima* but with an additional focus on the effects of turbulent flow at blade scales. Model experiments were also conducted by Vettori and Nikora (2018) employing single blades of polyethylene as a proxy material with drag force also represented in a unidirectional form.

In this study, the unidirectional representation of hydrodynamic force is expanded to resolve normal and tangential components of drag on aggregates of kelp. Since the angle between the compliant kelp material and the fluid velocity vector can change in a dynamic flow regime, determining each component is necessary to calculate instantaneous, time-averaged, and maximum drag on the kelp in unsteady flows. Furthermore in aquaculture applications, yield of seeded sugar kelp can be 8 kg/m (Kim et al., 2015) to values exceeding 17 kg/m while having over 330 plants per meter (Augyte et al., 2017).

The hydrodynamics of dense aggregates of kelp may have implications beyond the single blade dynamics. Therefore, the objective of this study was to characterize the components of drag force on a full- scale model having numerous kelp blades. A robust proxy model was designed to represent the attributes of kelp grown at a University of New England experimental aquaculture lease site in Saco Bay, Maine in the USA. Tow tank experiments were conducted at the United States Naval Academy (USNA). Tow tank test results yielded a set of normal and tangential drag-area values relative to component velocities. With the force components, a threshold point was determined representing the transition from normal to tangential drag dominance.

2. Methodology

2.1. Design of the physical model

2.1.1. Approach to determine geometric and material properties

To determine the hydrodynamic characteristics of a section of densely grown kelp, a comprehensive set of towing tank experiments were performed using a full-scale physical model. The design of the physical model was based on the nominal characteristics of *S. latissima* cultivated on a 60 m kelp line in Saco Bay, Maine, USA (Fig. 1a). The seeded line was deployed in November 2015 and harvested in early May 2016 yielding kelp up to 3 m in length with an estimated 15 kg of biomass per meter of line (Fig. 1b). With this level of biomass, it was clear that the model would have to incorporate numerous blades, an exact number not known at the time but to include up to 330 per meter as recently cited in Augyte et al. (2017). Buck and Buchholz (2005) did performed tow tests with a clump of 13 blades, but used samples of actual kelp. In the present study, the goal was to build a robust proxy model maximizing the number of blades to best represent the yield found in Saco Bay. A full-scale, proxy model approach was chosen to reduce issues associated with dynamic similarity and to acquire experimental replicates difficult to obtain with actual kelp due to material degradation.

When this study was initiated, *S. latissima* product from the Saco Bay aquaculture site was unavailable as it was out of season. Therefore, three samples of wild kelp were collected from Saco Bay to supplement six cultured samples obtained from a nearby farm to the north. The intent was to represent a range of kelp flexural rigidity and mass density (ρ_{kelp}) values described by Stewart (2006) and Luhar and Nepf (2011) as dominant material response parameters. Flexural rigidity was defined as EI with the modulus of elasticity (E) multiplied by the second area moment of the cross-section (I). The mass density was defined simply as the mass (m) of a sample divided by its volume (V). Both the wild and farm samples were kept in flowing seawater.

Cantilever beam tests were performed within a day of collection (minimizing deterioration) to determine the flexural rigidity of the samples assuming the material under its own weight was linear elastic. Since it was imperative that the tests be done immediately, the simple beam test (Demes et al., 2011) was employed acknowledging that the technique assumes a stiff cross section. From mechanics of materials (e.g. Goodno and Gere, 2020), the flexural rigidity of a blade sample (δ_{blade}) was therefore estimated from

$$Flexural\ Rigidity = EI = \frac{wl^4}{8\delta_{blade}} \tag{1}$$

with l as the length of the deflected portion of the sample from its distributed weight (w)

$$w = \frac{\rho_{kelp} g V}{l} \tag{2}$$

Obtaining the second area moment values of the kelp samples was an issue since cross-sectional area characteristics were not regular shapes, a concern described in Rominger and Nepf (2014). To simplify the approach, it was assumed that the stiffest part was a rectangular section within the meristematic portion of the blade, from which samples were cut with a rectangular cross section,

$$I_{Cross-section} = \frac{1}{12} b t^3, \tag{3}$$

where b is the width and t is the thickness of the sample.

From the field collected kelp, the length (L) and width (b) were measured on each side and averaged. The thickness (t) of the sample was measured at 8 locations that included the corners and midpoint positions, and were also averaged. The volume (V) was then calculated and the mass of each of the samples measured and used to calculate the mass density (ρ_{kelp}), from which the weight per length (w) of each sample was determined with Eq. (2). It is important to note that the wetness of the sample is a strong source variability with this approach. Therefore it was decided to keep the actual kelp samples "wet" but not dripping prior to taking measurements. Eq. (3) was used to find the second area moment (I) with the cross-sectional dimensions. The cantilever beam test was performed to measure the deflection (δ_{blade}) as a function of the distributed weight with the EI values calculated using Eq. (1). Knowing the second area moment (I) of the sample, the modulus of elasticity was then estimated. Resulting values were compared with those published in Section 3.1.1.

2.1.2. Kelp aggregate model design parameters

The design of the kelp aggregate for the tow experiments considered several proxy material types including various elastomers such as chloroprene (neoprene), isobutene-isoprene (butyl), and polyurethane rubber. Other materials such as polyvinyl chloride film and flat polyethylene, plastic tubes were also considered. Flexural rigidity (EI) for each of the materials was calculated based on manufacturer specifications. Once the proxy material was chosen, the EI was verified using the Peirce (1930) method with a plane angle of 41.5° as applied by Henry (2014) for macroalgae. With the proxy material, the design of the full -scale kelp aggregate model was built based on the (1) exposed length, (2) individual blade flexural rigidity, (3) maximum number of blades per unit width that could fit on the mount, (4) mass/length of biomass and (5) the aggregate mass density.

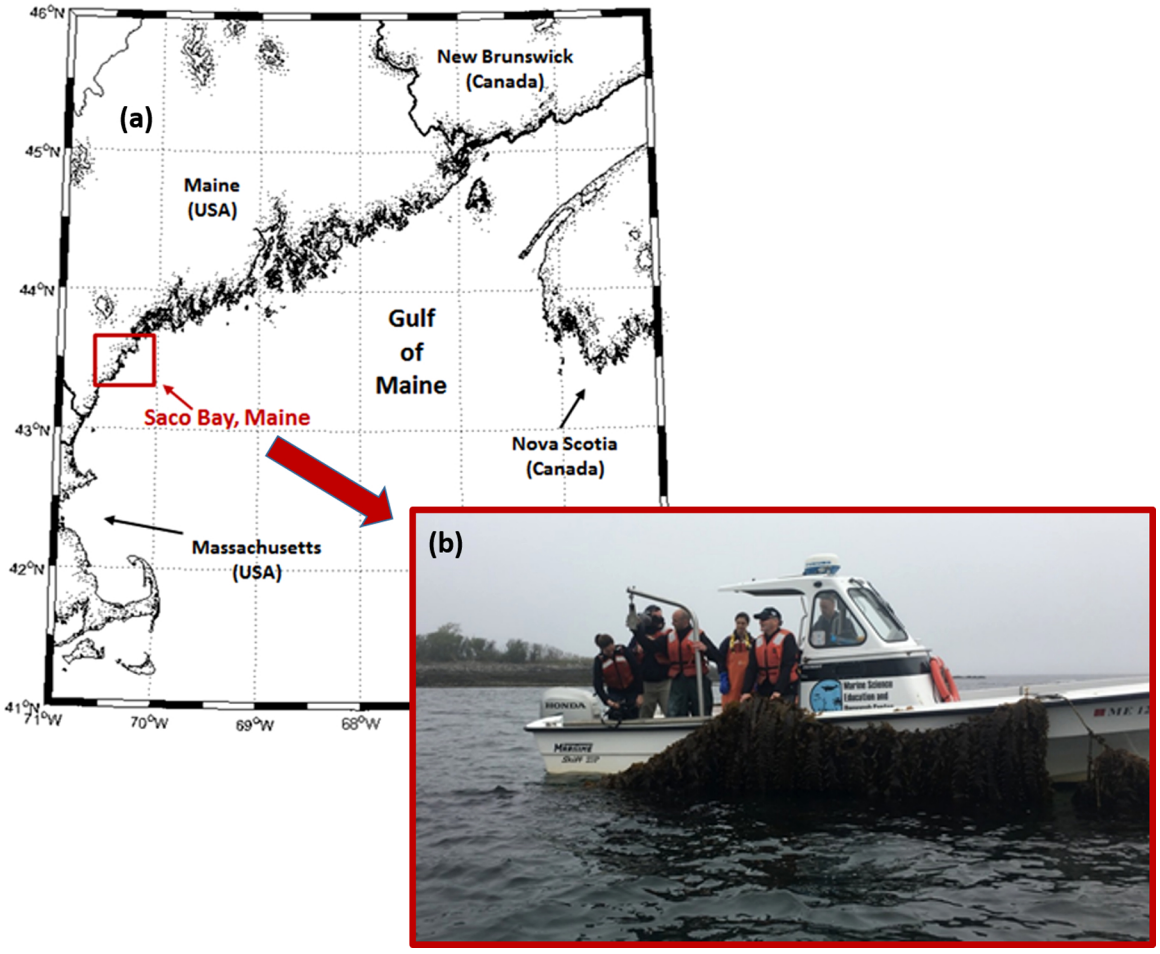

Fig. 1. (a) Saco Bay, Maine (USA) is located in the western Gulf of Maine. (b) In 2016, the kelp line in Saco Bay was harvested at an estimated biomass of 15 kg/m.

2.2. Tow experiments

2.2.1. Experimental setup

The tow experiments were conducted in the Hydromechanics Laboratory at the USNA in a fresh water basin with the dimensions of 116m × 7.9m × 4.9 m. The large tank size enabled the use of full-scale models. Two models were constructed, one with mounted-kelp and the other representing a tare (mounted-tare). The tow carriage mount configurations are show in Fig. 2. The mounted-kelp and -tare models were attached to the tow carriage with vertical struts and force blocks to measure both horizontal and vertical forces. Two sets of tests were conducted with the models. The first tests were done with the mounted-kelp and -tare models aligned to the direction of the tow and the second tests were done with the models perpendicular to the direction of the tow. During the experiments, the carriage was towed the length of the tank at increasing speeds of 0.25, 0.50, 0.75, 1.00 and 1.25 m/s. Ten replicate datasets from the horizontally mounted force block were obtained for the aligned and eleven replicate datasets were obtained for the perpendicular orientations.

As described in Fredriksson et al. (2010), each force block consisted of a 102 mm "block" made of ARMCO 17 − 4PH stainless steel with flexures sensitive to forces along one axis. Motion is sensed by a waterproof, variable reluctance displacement transducer powered by a Validyne CD 19A amplifier. The amplifier produces an analog DC voltage (10 V) that is proportional to the force applied to the gage. The voltage is sampled with a 16 bit PC-based analog-to-digital system at 50 Hz. Each force block was calibrated at the Hydromechanics Laboratory at the USNA to a full-scale load of 178 N. The standard

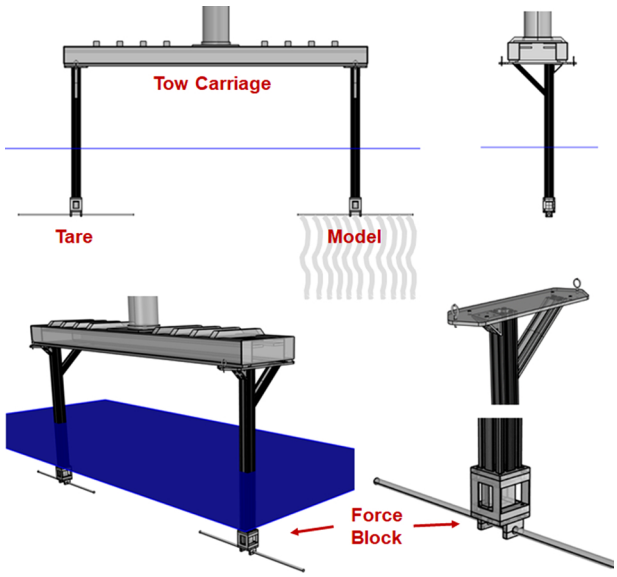

Fig. 2. Both the mounted-kelp and -tare models were attached to a vertical strut with force block transducers and connected to the towing carriage in the large tow tank facility at the U.S. Naval Academy. The vertical force block is not shown on the figure.

instrumentation bias of the force block instruments are 0.25% of the full calibrated load equal to 0.445 N.

2.2.2. Uncertainty estimates

Uncertainty estimates of the velocity dependent force block measurements followed the approach described in Schultz (2005) done for tow tank datasets. In this approach, two-tailed t_s values were obtained (Coleman and Steele, 1995) at the 95% confidence level for degree of freedom values of 9 and 10 for the aligned and perpendicular tow orientations, therefore yielding t_s values of 2.228 and 2.262, respectively. Degree of freedom values were taken as one less than the number of replicates (n) for each set of tests. With the t_s values, measurement precision was calculated as the standard error of the mean

$$\textit{Measurement Precision} = \frac{\left\{\sqrt{\frac{\sum(f_i - \overline{F})^2}{n-1}}\right\} t_s}{\sqrt{n}} \quad (4)$$

where f_i are the force block values and $\overline{F}$ as the mean. Instrument bias values were taken as standard from the manufacturer as 0.445 N (Section 2.2.1). Total error was estimated from the root of the measurement precision and instrument bias squares as described in Moffat (1988).

2.2.3. Force balance and coordinate transformation

During the tow tests, horizontal and vertical reaction forces were measured with the force blocks at each model attachment shown in Fig. 3(a) and (b). To resolve the normal and tangential drag components on the flexible structure from the measured forces, force balance and coordinate transformations calculations were conducted. In this procedure, a global coordinate system was set at the attachment location such that the *X*-axis was aligned with the attachment bar and the *Y*-axis perpendicular to the attachment bar with the forces measured along each axis defined as F_X and F_Y, respectively. This orientation was chosen to be similar to the definition by Faltisen (1991) with respect to moving ships. During the tow tests, three replicates were obtained from the force block mounted at a 90 degree angle to measure vertical forces upwards. This was defined as the *Z*-axis. Since a set of vertical forces were measured for both the aligned and perpendicular orientation, the datasets were defined as F_{Za} and F_{Zp}, respectively (also shown in Fig. 3(a) and (b).

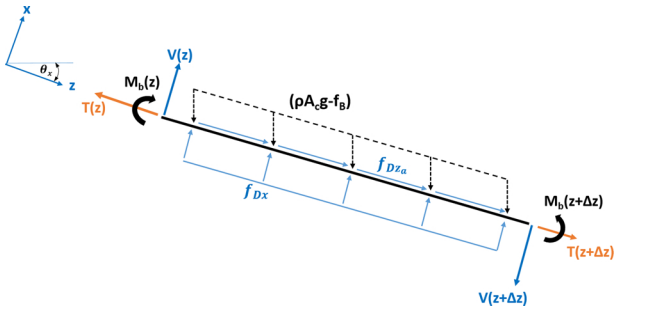

Fig. 4. Force balance diagram of a beam section of the physical model away from the attachment point and the free end. At steady state, resolving the force balance in the local x-direction yields the normal drag force per unit length. The force balance in the y-z plane is orthogonal and identical.

Force balances were then defined (Fig. 4) for a local section of the kelp model away from the attachment point and the free end in steady flow. Since no curvature was observed at this midpoint section during the tests, the shear force (V) and bending moment (M_b) in this region of the aggregate were assumed to be zero. Defining the diagram with a local coordinate system having the x-axis normal and the z-axis tangential to the aggregate (x–z plane), the force balance resolves the normal component of drag (f_{Dx}) per unit length as

$$f_{Dx} = (\rho_{aggregate} A_c g - f_B)\cos(\theta_x) \quad (5)$$

with $\rho_{aggregate}$ as the mass density of the composite aggregate material, f_B is the buoyant force per length and θ_x as the angle from the horizontal. Since the normal drag force is distributed, per unit length on a section of the model, A_c is the cross sectional area of the aggregate based only on volume. The same approach was applied in the *y*–*z* plane,

$$f_{Dy} = (\rho_{aggregate} A_c g - f_B)\cos(\theta_y) \quad (6)$$

with θ_y as the corresponding angle from the horizontal.

This force balance approach, however, could not resolve the tangential per unit length components (f_{Dz_a} *and* f_{Dz_p}) since the local tension (T) along the aggregate could not be measured. Instead, the total tangential drag forces (F_{Dz_a} and F_{Dz_p}) were determined with a force

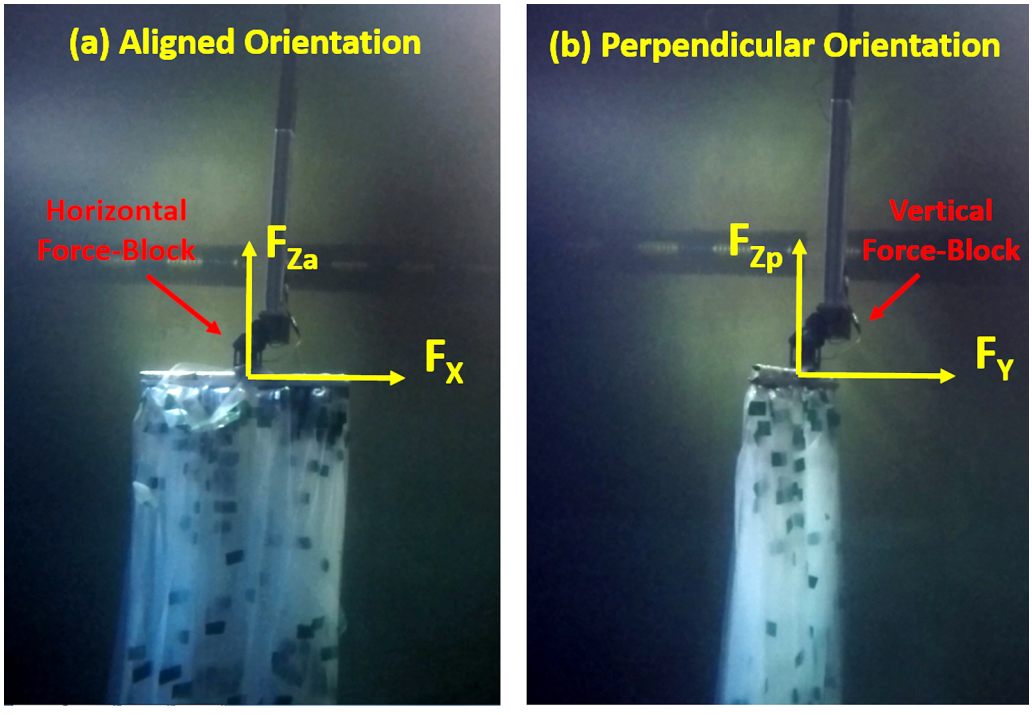

Fig. 3. Tests were conducted in aligned (a) and perpendicular (b) orientations with respect to the centerline of the tank. The coordinate system of *X*, *Y* and *Z* were defined by the orientation of the kelp-model attachment bar with the aligned axis as *X* and the perpendicular axis as *Y* to obtain the F_X, F_Y. The corresponding vertical components were defined as F_{Za} and F_{Zp} for the aligned and perpendicular sets of measurements.

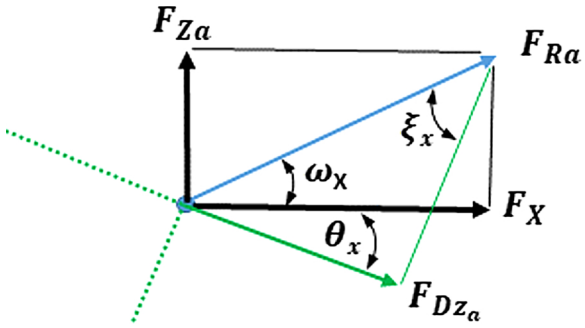

Fig. 5. Transformation of coordinates to calculate F_{Dz_a} from the measured F_X and F_{Z_a} forces. The coordinate transformation in the *Y–Z* plane is orthogonal and identical.

transformation (Fig. 5) from the resultants (F_{Ra} and F_{Rp}) of the force block measurements and corresponding angles (ω_X and ω_Y),

$$F_{Ra} = \sqrt{F_X^2 + F_{Za}^2}, \tag{7}$$

and

$$\omega_X = arctan\left(\frac{F_{Za}}{F_X}\right) \tag{8}$$

$$F_{Rp} = \sqrt{F_Y^2 + F_{Zp}^2} \tag{9}$$

and

$$\omega_Y = \arctan\left(\frac{F_{Zp}}{F_Y}\right) \tag{10}$$

Then coordinate transformation was done with

$$\xi_x = \frac{\pi}{2} - \omega_X - \theta_x \tag{11}$$

And

$$\xi_y = \frac{\pi}{2} - \omega_Y - \theta_y \tag{12}$$

also shown in Fig. 5. The tangential forces (F_{Dz_a} and F_{Dz_p}) were then calculated and converted to per unit length of kelp model (L_{kelp} = 3 m) along the blade axis for the aligned and perpendicular orientations with

$$f_{Dz_a} = \frac{F_{Dz_a}}{L_{kelp}} = \frac{F_{Ra} sin(\xi_x)}{L_{kelp}} \tag{13}$$

and

$$f_{Dz_p} = \frac{F_{Dz_p}}{L_{kelp}} = \frac{F_{Rp} sin(\xi_y)}{L_{kelp}}. \tag{14}$$

2.2.4. Data analysis

Each tow test included the five speeds running the length of the tank for about 110 s. Time series datasets for each speed were obtained for approximately 20 s. Acceleration of the tow carriage between each speed took about 2 s, from which steady state conditions from the force block measurements were achieved after 4 s. For each setting, force and tow speed pairs were obtained by time averaging approximately 10 s of the steady-state values assuming the tow segment was a stationary process. Representative values at each speed were then ensemble averaged assuming ergodicity. With the ensemble averages, the mounted-tare values were subtracted from the mounted-kelp values to obtain kelp-only F_X, F_Y, F_{Za} and F_{Zp} in the aligned, perpendicular and vertical orientations, respectively. The force blocks were set to zero at the beginning of each tow so the wet weight of the mounted-kelp and -tare values were removed from the F_{Za} and F_{Zp} datasets. This was done to isolate the hydrodynamic forces, especially in the vertical direction since the wet weight had been measured.

In addition to the force datasets, digitized video was also captured to quantify the deflected angle of the compliant kelp model. Individual frames at each speed were used to measure the deflected angle scaled within a computer aided design (CAD) program when steady state conditions were achieved. The deflected angle was measured down from the horizontal axis of the global coordinate system to a line parallel to the leading edge of the kelp model aggregate.

With the datasets obtained from the force blocks, normal and tangential drag force components on the model kelp aggregate were determined. Drag force representations can take multiple forms for submerged, compliant macrophytes (Statzner et al., 2006) similar to *S. latissima*. In this case, normal and tangential drag forces were used to calculate the corresponding drag-area (Hoerner, 1965) for each component. This approach was taken because reference areas were ambiguous since not all blades were 100% exposed to the flow, similar to observations of cultured kelp in Saco Bay (see Fig. 13 in Section 4.1). The drag-area values, per unit length of kelp model, were calculated as

$$s_{Dx} = \frac{(f_{Dx})}{\frac{1}{2}\rho_w {U_x}^2}, \tag{15}$$

$$s_{Dz_a} = \frac{(f_{Dz_a})}{\frac{1}{2}\rho_w {U_{z_a}}^2}, \tag{16}$$

$$s_{Dy} = \frac{(f_{Dy})}{\frac{1}{2}\rho_w {U_y}^2} \tag{17}$$

and

$$s_{Dz_p} = \frac{(f_{Dz_p})}{\frac{1}{2}\rho_w {U_{z_p}}^2}, \tag{18}$$

with units of length. If a reference area and length can be defined, non-dimensional drag coefficients can be calculated from the drag-area values.

In Eqs. (15)–(18),

$$U_x = Usin(\theta_x) \tag{19}$$

and

$$U_{z_a} = Ucos(\theta_x) \tag{20}$$

are obtained from the aligned orientation, while

$$U_y = Ucos(\theta_y) \tag{21}$$

and

$$U_{z_p} = Usin(\theta_y) \tag{22}$$

are obtained from the perpendicular orientation. Representing drag in this manner with relative component velocities is consistent with approaches described in Casarella and Parsons (1970) which is necessary for calculating drag in unsteady flows and for use with configurations not tested in the tank.

3. Results

3.1. Kelp aggregate model final design

3.1.1. Proxy material

From the wild and cultured kelp, rectangular sections were cut from the two sets of samples. The average length, width and thickness values for the wild samples were 13.85 ± 0.06, 6.12 ± 0.14 and 0.11 ± 0.01 cm. The average length, width and thickness values of the cultured samples were 12.95 ± 0.09, 2.34 ± 0.06 and 0.04 ± 0.01 cm. With each of the samples "wet but not dripping," the mass density characteristics were bracketed between 1.46 ± 0.04 and 1.26 ± 0.27 g/cm^3 for the wild and cultured kelp samples, respectively, with the results provided in

Table 1
Average geometric and material properties with standard deviation values measured from the *S. latissima* samples and physical model.

Parameter (average values)	Wild samples	Cultured samples	Physical model characteristics
Number of samples	3	6	10
Length (cm)	13.85 ± 0.06	12.95 ± 0.09	25.54 ± 0.14
Width (cm)	6.12 ± 0.14	2.34 ± 0.060	7.41 ± 0.05
Thickness (cm)	0.11 ± 0.01	0.04 ± 0.01	0.0213 ± 0.004
Volume (cm^3)	9.60 ± 0.29	1.17 ± 0.24	4.03 ± 0.07
Second area moment (cm^4)	7.44 ± 0.93 (10^{-4})	1.25 ± 0.1 (10^{-5})	5.97 ± 0.30 (10^-6)
Mass (gram)	14 ± 1	1.44 ± 0.22	3.66 ± 0.05
Mass density (g/cm^3)	1.46 ± 0.04	1.26 ± 0.27	0.900, LDPE 1.379, Model
w (N/m)	0.99 ± 0.01	0.11 ± 0.02	0.141 ± 0.01
Flexural Rigidity (Nm^2)	7.86 ± 1.77 (10^{-5})	1.31 ± 0.20 (10^{-7})	2.19 ± 0.38 (10^{-5})
Modulus of Elasticity (MPa)	10.58 ± 0.20	1.28 ± 0.43	367 ± 63

Table 1. Though not known at the time, these values were higher than those measured at 1.092 ± 0.091 g/cm^3 by Vettori and Nikora (2017). The flexural-rigidity results (EI) represented a range of 2 orders of magnitude, 7.86 ± 1.77 (10^{-5}) and 1.31 ± 0.20 (10^{-7}) Nm^2 (Table 1), but was expected since the wild samples were much more robust than the delicate cultured samples. The modulus of elasticity values derived from the cantilever beam tests had a tighter range with values between 10.58 ± 0.20 and 1.28 ± 0.49 MPa (also provided in Table 1). These results were similar to Vettori and Nikora (2017) for *S. latissimi* with modulus of elasticity values of 3.73 ± 2.71 and 4.71 ± 1.81 MPa using two independent techniques. The first value cited by Vettori and Nikora (2017) was acquired with the Peirce (1930) methodology derived for flexible cross-sections, and the second value with linear elastic stress/strain experiments.

Based on this field information, candidate material types as described in Section 2.1.2, along with size and amount available were examined. Since it was chosen to build the model to be representative of kelp at high yield (15 kg/m), numerous lengths of proxy material for the full-scale model tests was needed. It was found that 6 mil (t = 0.02 cm), low density polyethylene (LDPE) flat tubing with a nominal width of 7.62 cm had the best potential for matching the flexibility characteristics while obtaining the amount needed since it could be purchased in 152 m rolls. Ten samples were cut with a length, width and thickness of 25.54 ± 0.14, 7.41 ± 0.05 and 0.0213 ± 0.004 cm, respectively. The volume, second area moment and mass values of the samples were obtained with results provided in Table 1. The mass density was calculated at 0.900 g/cm^3 similar to standard values ranging from 0.912 – 0.955 and a mean of 0.923 g/cm^3 (www.matweb.com). Note that the mass density would have to be increased to match that of the actual kelp samples. From the same material source, modulus of elasticity values are published with a range of 190–520, with a mean of 320 MPa. With such a large range, the modulus of elasticity value was verified experimentally by first obtaining EI using the Peirce (1930) method with a plane angle of 41.5°. This yielded a value of 2.19 (10^{-5}) Nm^2 which was within the range of the wild and cultured kelp samples. With the experimental EI value and the measured second area moment, the modulus of elasticity was then calculated to be 367 MPa, comparing well with published values.

Recent work has also shown that choosing the proxy material with a rectangular shape has similarities to exposed condition morphology. In particular, the cultured kelp samples collected as part of this study has since been characterized as "skinny kelp" by Augyte et al. (2017) that typically grows in a distinct exposed environment at a nearby Maine

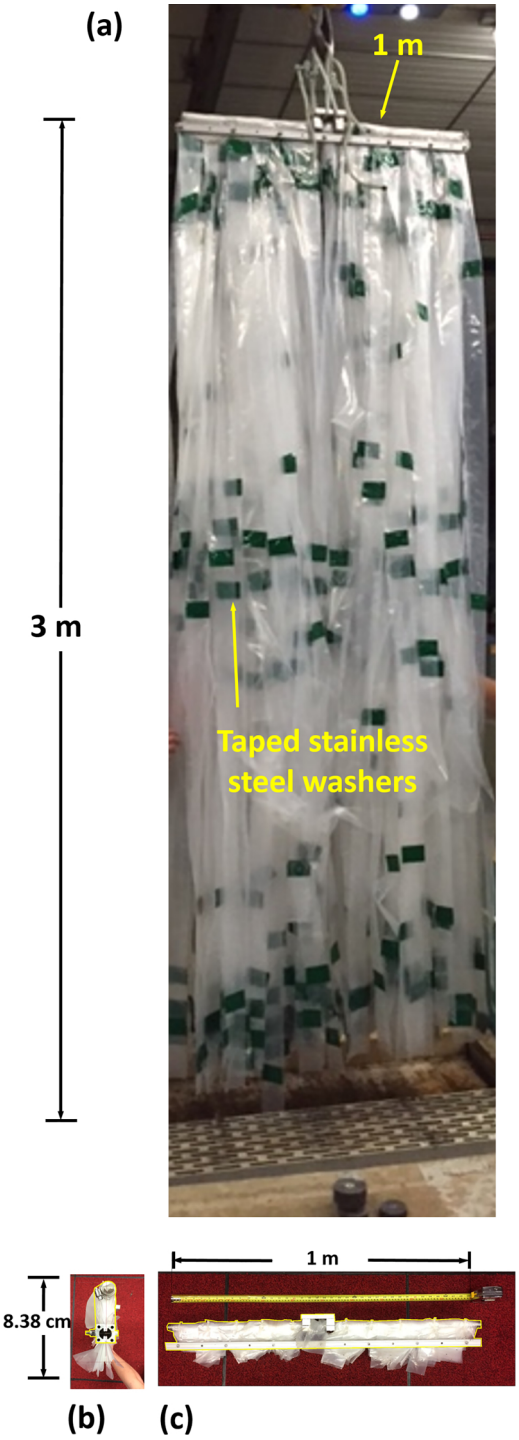

Fig. 6. (a) The full-scale, mounted-kelp model with the dimensions of 1 m × 3m and with a dry mass of model blades equal to 16.11 kg. To achieve the dry mass requirement, three stainless steel washers were taped to the strips. (b) A side view of the mounted-tare model and (c) the front view of the mounted-tare model.

site. It is generally described as having flat blades with lengths between 1.8–4.4 m, widths 1.6–5.0 cm, and thicknesses from 1.1 to 1.5 mm, terming the morphotype "*Saccharina latissima forma angustissima*." With further genetic analysis and field experimentation, Augyte et al. (2018) claimed enough differentiation to warrant speciation as *Saccharina angustissima,* though *S. angustissima* and *S. latissima* are able to freely hybridize in a laboratory setting. *S. angustissima* likely represents an extreme in phenotypic plasticity and therefore supports the assumption

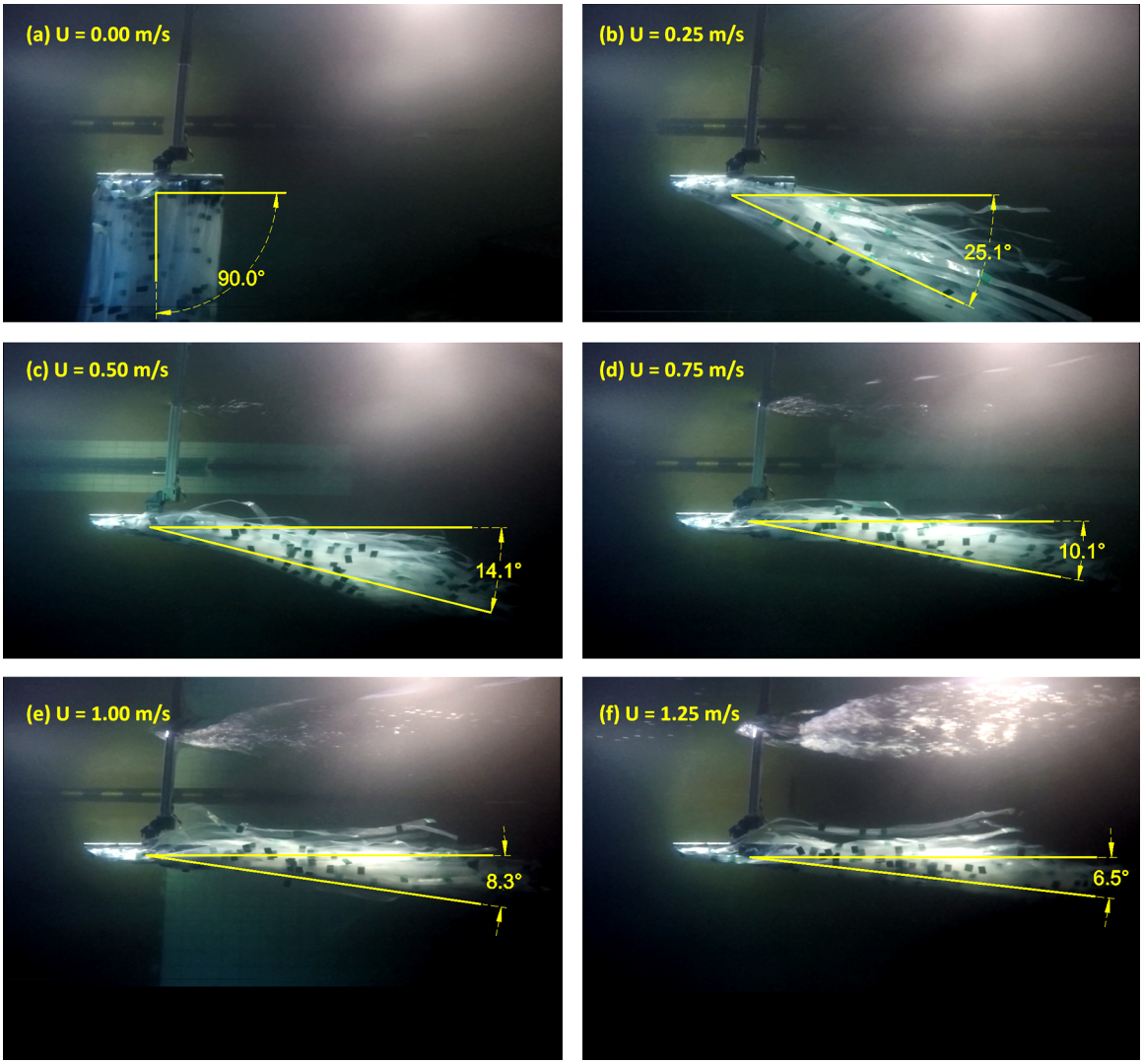

Fig. 7. Deflected angle θ_x for the aligned orientation at each of the five towing speeds.

that the samples originally obtained represent the more flexible range of potential characteristics. The exposed kelp found by Buck and Buchholz (2005) was described in a similar manner with blades being more streamlined, having few undulations along the fringes. The geometry was represented as a ratio between blade length and width with three distinct growth phases such that with lengths greater than 2 m, the width of the kelp was nominally 20 cm. The LDPE proxy model fit with these two similar exposed site morphologies. With the proxy material, the design of the full-scale kelp aggregate model was built based on the (1) exposed length, (2) individual blade flexural rigidity, (3) maximum number of blades per unit width that could fit on the mount, (4) mass/length of biomass, and (5) the aggregate mass density.

3.1.2. Kelp aggregate model specifications

With the kelp proxy material chosen as LDPE, the design items described in Section 2.1.2 were addressed. The model length (item 1) was set to 3 m based on maximum values from the kelp line shown in Fig. 1. The individual blade flexural rigidity (2) was discussed in Section 3.1.1 and having the values provided in Table 1 where LDPE tube was found to be in the range of the samples measured at that time. The model width was set at 1 m for which it was found that 178 plastic strips could fit on the mounting bar, maximizing item (3) though still less than found *in-situ*. To increase the mass density, three stainless steel washers were added to the top, middle and bottom sections of the 3-meter strips of LDPE. Point masses were used to minimize the influence on the flexural rigidity of the LDPE. Mass values were first determined with 10 individual strips fabricated with washers and tape obtaining a value for each blade equal to 88 ± 1.9 g. With 178 plastic blades fitting on the 1 m bar, the total mass of the aggregate model was estimated from the 10 samples as 15.66 kg (satisfying item 4). This required 534 m of LDPE plastic tube. Once all 178 of the model blades were completed, the mass of the entire aggregate was verified from measured mass values both in and out of water as 4.45 and 16.11 kg. By knowing that the tank water mass density was 997.7 kg/m^3, the volume of the aggregate was determined as 0.01167 m^3. Then the mass density of the model aggregate (item 5) was calculated at 1379 ± 20 kg/m^3 ($\rho_{aggregate}$). A mount was then attached to the rod for the force blocks. The 1m × 3m mounted-kelp model is shown suspended from a crane in Fig. 6 (a). In addition to the full-scale, mounted-kelp model, a second model representing the mounted-tare, was also built. Aligned and perpendicular views of the tare are shown in Fig. 6(b) and (c) showing an 8.38 cm distance between the rod and the clamp to secure the LDPE strips. The mounted-tare included the same bar, clamp and force block mount with 178 shortened plastic strips. The shortened plastic strips were included with the bar clamp since the clamp was needed for the mounted-kelp model. The shortened plastic strips were also included in an effort to decouple the hydrodynamic influence of the rigid mount when removing the hydrodynamic drag measurements of the mounted-

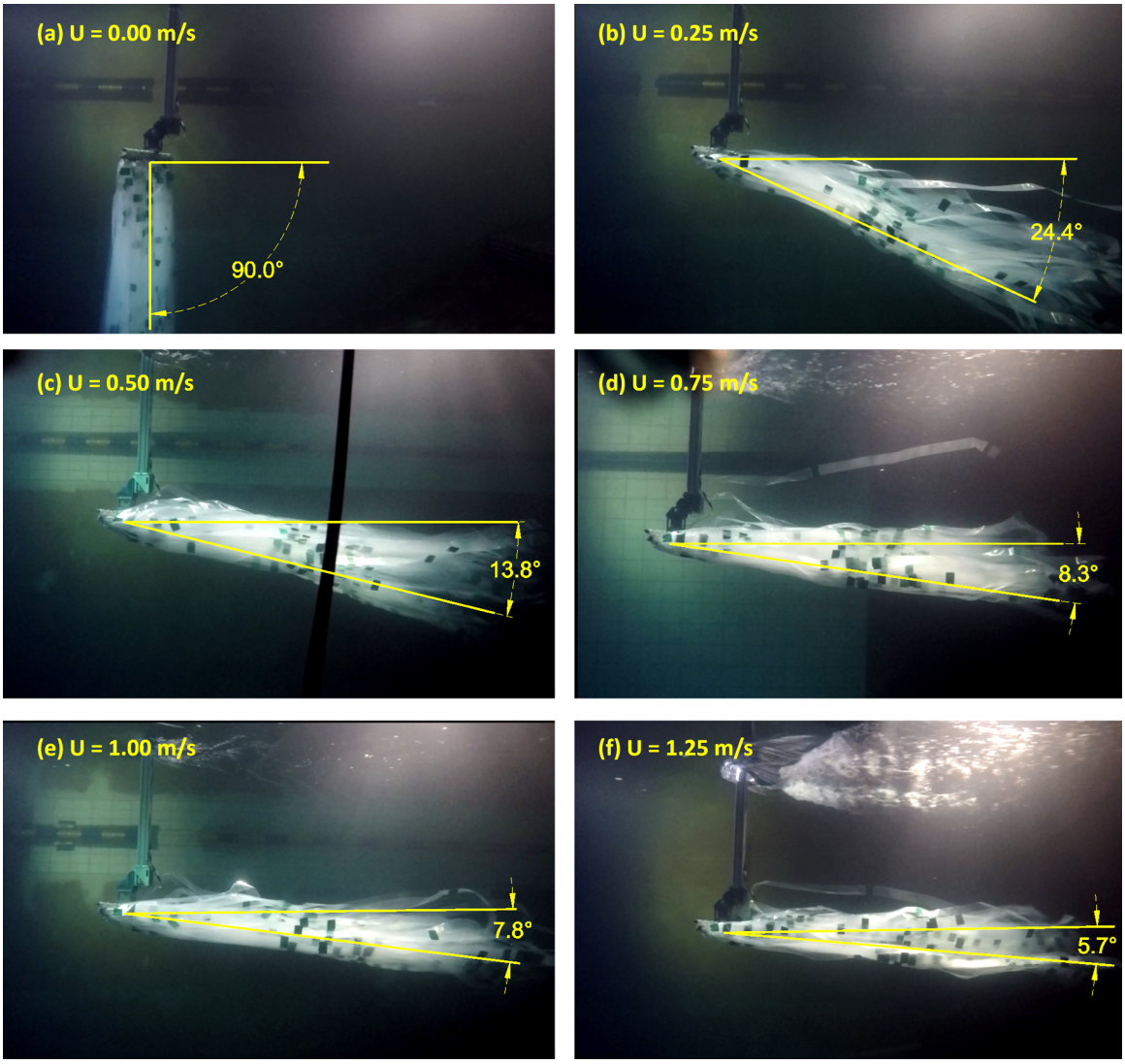

Fig. 8. Deflected angle θ_y for the perpendicular orientation at each of the five towing speeds.

tare from the mounted-kelp model to obtain kelp-only datasets.

Additional field datasets have been collected at the Saco Bay site since the 2015–2016 season that further justifies the number of LDPE proxy model strips. For example, during the harvest of 2018, samples were taken from cultured kelp to characterize yield. Results of sampling from two, 10 cm locations yielded 43 and 49 blades, respectively. In April of 2019, a value of 35 blades was found on a 10 cm section at the same site further distinguishing the yield of the aquaculture system from single blade experiments and supporting the technique to maximize the number of blades, as practically possible, used on the model.

3.2. Towing experiments

3.2.1. Deflection angles

As described in Section 2.2.4, the model kelp aggregate angle at each speed was estimated from a captured video frame during the steady-state portion of the tow and quantified with a CAD program. The results (θ_x and θ_y) are shown in Figs. 7 and 8 for the aligned and perpendicular orientations respectively. The figures show the angles formed at each origin (defined in Figs. 4 and 5) from the horizontal axis to a line parallel to the leading edge of the aggregate. Deflected angle values, θ_x and θ_y, were similar with differences of 0.7, 0.3, 1.8, 0.5 and 0.8 degrees at each of the increasing speeds between the orientations. The Figures also show the reconfiguration of the kelp aggregate model with increasing speed with the largest change occurring between 0 and 0.25 m/s.

3.2.2. Drag force and area results

From the horizontally mounted force blocks, ensemble averages were calculated from the 10 and 11 replicate datasets for the aligned and perpendicular orientations to obtain the mounted-kelp and –tare results as shown in Fig. 9(a) and (b). The mounted-kelp and –tare datasets were then processed to obtain kelp-only, F_X and F_Y results representing both orientations as shown in Fig. 9(c). The mounted-kelp and –tare total error values (eqn. 4) were then determined using the methodology described in Section 2.2.2 with results provided in Table 2.

The mounted-kelp and –tare datasets for each orientation show force differences due mostly to the frontal area of the mount. When this component is removed, the kelp-only datasets in Fig. 9 (c) for each orientation show similarities at speeds between 0.25 and 0.75. At speeds greater than 0.75, the results in the perpendicular orientation (F_Y) increase more than those in the aligned orientation (F_X). One possible explanation is that the aligned shape becomes more streamlined with less area from 178 blades exposed to the flow. The blades associated with the perpendicular orientation, seem to maintain side-view shape and exposed area with increasing speed. The results from both orientations in Fig. 9 (c) indicate that there must exist an inflection

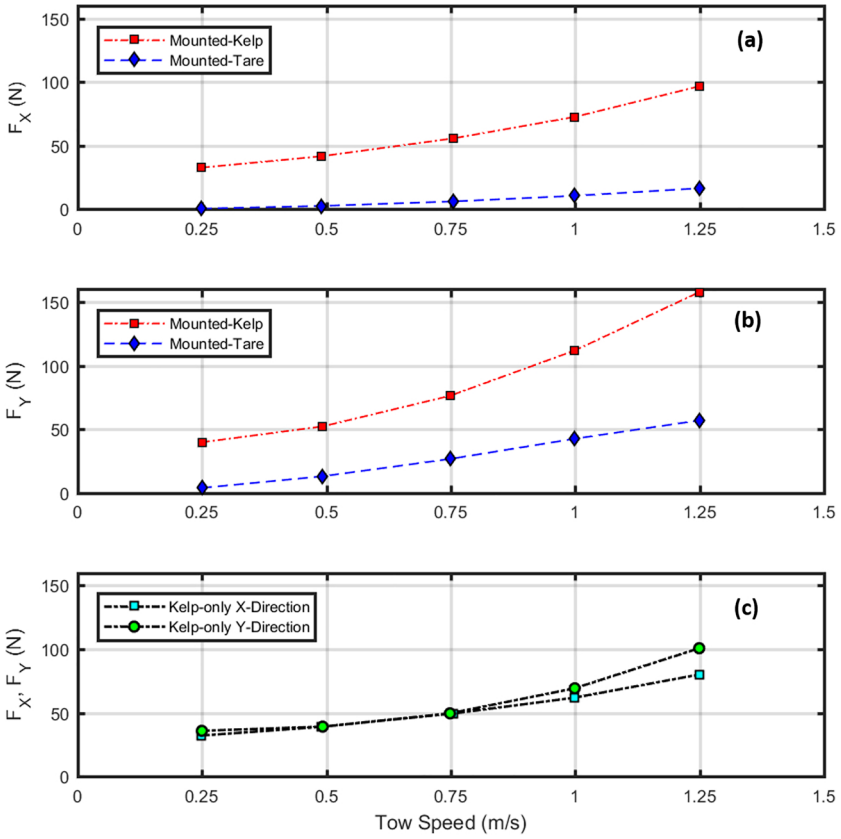

Fig. 9. The horizontal force results in the *X*- (a) and *Y*-directions (b) associated with the aligned and perpendicular orientations, respectively. The kelp-only datasets are shown in (c). Both datasets in (c) suggest a transition from 0 to 0.25 m/s due to the kelp aggregate becoming more streamlined.

Table 2
Horizontal force mean value and total error results for the mounted-kelp and -tare configurations.

Nominal tow speed (m/s)	Aligned orientation				Perpendicular orientation			
	Mounted-kelp (N)		Mounted-tare (N)		Mounted-kelp (N)		Mounted-tare (N)	
	Mean	Total error	Mean	Total error	Mean	Total error	Mean	Total error
0.25	32.72	1.872	0.56	0.492	39.77	1.612	3.90	0.691
0.50	41.60	2.406	2.61	0.527	52.23	1.511	13.05	2.054
0.75	55.72	2.94	6.18	0.650	76.25	2.049	26.64	3.790
1.00	72.53	3.80	10.59	1.075	111.82	3.580	42.54	4.387
1.25	96.66	4.334	16.51	1.546	157.67	4.933	56.93	5.233

point below 0.25 m/s for the drag to reach zero at 0 m/s.

As described in Section, a second force block was installed on both the mounted-kelp and –tare models for three of the towing tests in each orientation. The two additional force blocks were utilized to measure the vertical forces during the towing tests. Prior to initializing each tow, the vertical force blocks were also set to zero to remove the wet weight of the model to isolate the vertical hydrodynamic forces. The vertical forces were processed in the same manner as the horizontal forces. The mounted-kelp, mounted-tare and kelp-only results are shown in Fig. 10 (a) and (b). The Figures also include the estimated wet weight of the model (43.65 N) as a positive value for comparison with the measured vertical force. The difference between the measured vertical force and the wet weight shows that hydrodynamic force approaches, but never reaches a point of completely supporting the wet weight.

The hydrodynamic properties of the kelp model were obtained from the results of the tank tests by applying the force balance principles with the geometric and material properties (Section 2). With the deflected angles, the normal force components per unit length for the mounted-kelp model, f_{Dx} and f_{Dy}, were calculated based on the force balances in Eqs. (5) and (6). The F_{Za} and F_{Zp} forces for the mounted-kelp model were converted to the tangential components, f_{Dza} and f_{Dzp} by coordinate transformation from Eqs. (13) and (14) with the length of the kelp aggregate model. Drag-areas per length were then calculated from these force components using Eqs. (15)–(18). The force and drag-area results per unit length of kelp model are provided in Table 3.

4. Discussion

4.1. Transition from normal to tangential drag

The major result in support of the objectives was provided in Section 3.2.2 where drag forces on the model kelp aggregate were resolved into normal and tangential components. The components were obtained for both the aligned and perpendicular orientations related to the deflection angles (θ_x and θ_y). This expands on the unidirectional drag measurement approach of those cited in Section 1. The kelp-only datasets in Fig. 9 (c) show that the horizontal drag cannot be fit with a quadratic curve. Furthermore, it shows that there must exist an inflection point below 0.25 m/s for the drag to reach zero at 0 m/s. It is evident from Figs. 7 and 8 that the speed range from 0–0.25 m/s contains a transition from normal drag dominance to tangential drag dominance that is not captured in the horizontal drag only datasets. To investigate this transition that occurs in the lower speed regime for both orientations, the horizontal components of the normal and tangential drag forces were reconstructed with the results of the tow tests. First, the total horizontal force data values (F_X and F_Y) from Fig. 9 (c) were plotted per unit length as individual black diamonds in Fig. 11. Next, the horizontal components of the normal (f_{Dx} and f_{Dy}) and tangential

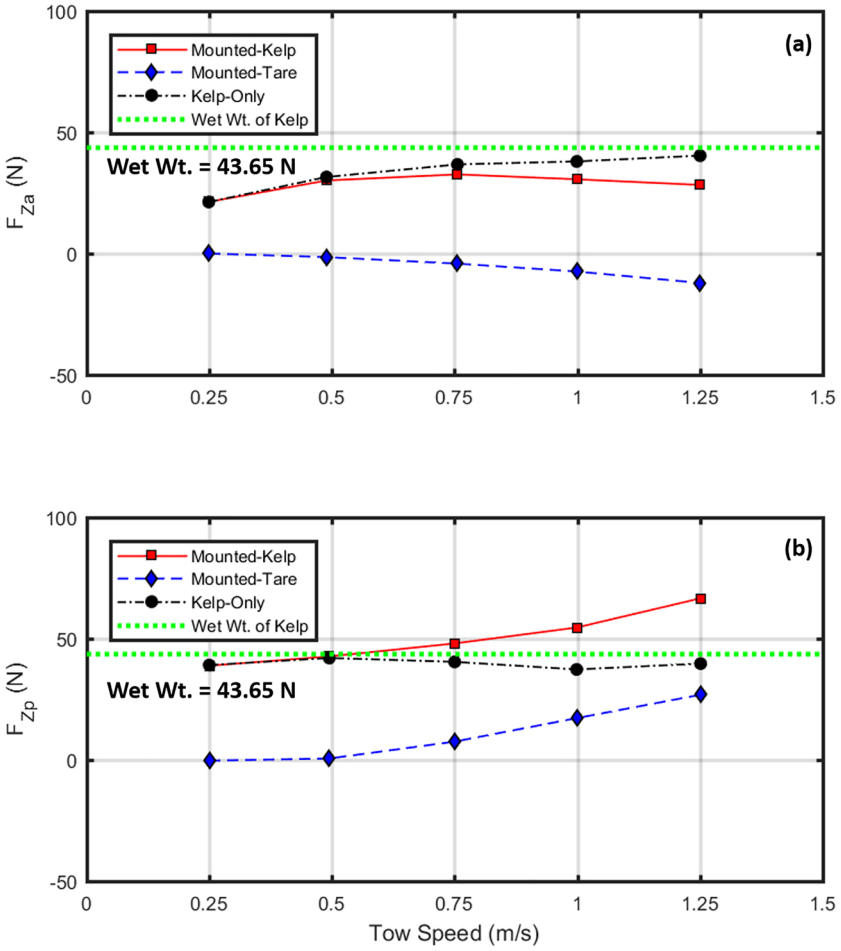

Fig. 10. The vertical force results in the aligned (a) and perpendicular (b) orientations. Also shown is the wet weight of the kelp-model as a positive value calculated as the difference between the dry weight and buoyancy equal to 43.65 N.

Table 3
Force and drag-area results per length of kelp model (L_{kelp} = 3 m).

Tow Speed (m/s)	f_{Dx} (N/m)	s_{Dx} (m^2/m)	f_{Dy} (N/m)	s_{Dy} (m^2/m)	f_{Dz_a} (N/m)	s_{Dz_a} (m^2/m)	f_{Dz_p} (N/m)	s_{Dz_p}(m^2/m)
0.25	13.18	2.36	13.25	2.49	6.70	0.2635	5.50	0.2125
0.50	14.11	1.99	14.13	2.04	10.04	0.0895	9.34	0.0812
0.75	14.33	1.64	14.40	2.46	14.11	0.0382	14.42	0.0525
1.00	14.40	1.39	14.42	1.57	18.60	0.0382	21.19	0.0434
1.25	14.46	1.45	14.48	1.88	25.02	0.0325	32.10	0.00415

(f_{Dz_a} and f_{Dz_p}) drag were obtained using the sine and cosine of the deflection angles and plotted as individual blue circles and red squares (also in Fig. 11), respectively. The sum of these components represent the total horizontal drag. These processed datasets show a possible intersection of the horizontal components of the normal and tangential drag forces near a speed of 0.25 m/s.

To construct the horizontal components for all tow velocities, including speeds less than 0.25 m/s, the normal drag-area values from Table 3 were linearly extrapolated as a function of the normal velocity component. The tangential drag-area values, however, were extraplolated as a power function of the tangential velocity component. Both sets of results are shown in Fig. 12. A system of simultaneous equations for each orientation was then created based on Eqs. (5) and (6) such that

$$0 = f_{Dx_i} - [\rho_{aggregate} A_c g - f_B] cos(\theta_{x_i}) \tag{23}$$

and

$$0 = f_{Dy_j} - [\rho_{aggregate} A_c g - f_B] cos(\theta_{y_j}). \tag{24}$$

This system of equations was iteratively solved for a set of deflection angles i and j. Note that f_{Dx_i} and f_{Dy_j} were also calculated from the velocity components obtained from the new set of angles and the drag-area values with Eqs. (15)–(22). With these computed values of normal and tangential drag, the horizontal components were determined and plotted in Fig. 11. The curves created from this system of equations show that at very low speeds, normal drag is the dominant contributor to the total drag. At a threshold near 0.25 m/s for both the aligned and perpendicular orientations, the horizontal component of tangential drag equals that of the normal drag. Above this reconfiguration threshold, tangential drag dominates. The sum of the computed components match the values measured from Fig. 9(c), but also include the transition not measured with the tow tests. The speed threshold is expected to be at slower speeds for kelp aggregates that are less dense than the model.

The transition from normal to tangential dominated drag is a

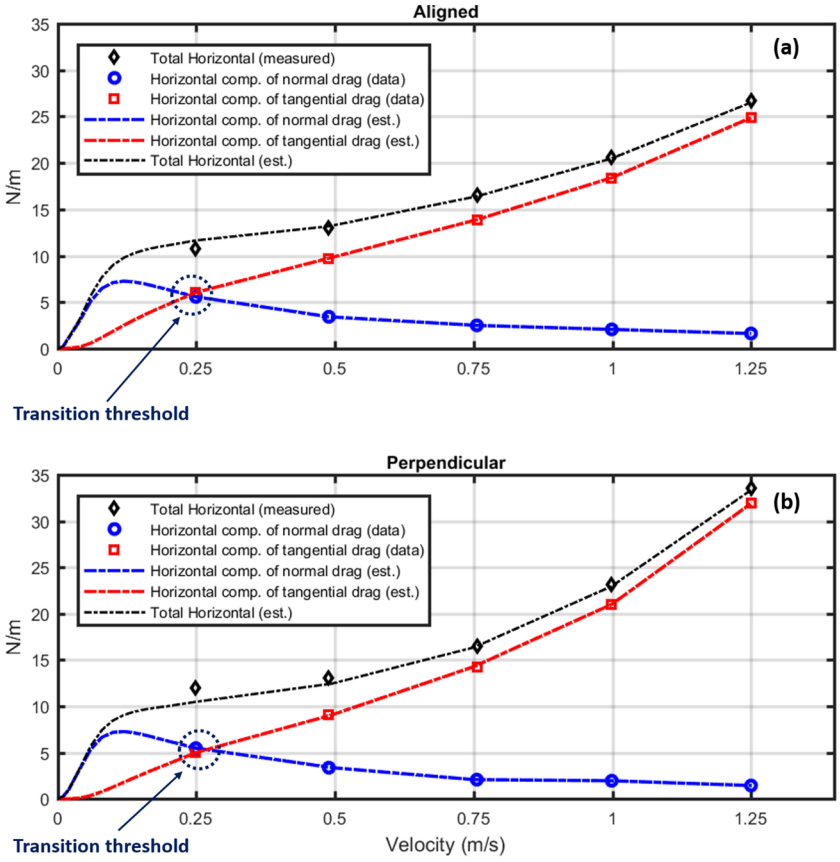

Fig. 11. The construction of the total horizontal force from the normal and tangential components using the derived drag-area datasets for both the aligned (a) and perpendicular (b) orientations. Drag-area values were extrapolated for speeds less than 0.25 m/s. The datasets yielded a transition threshold from normal to tangential drag dominance with increasing tow speed.

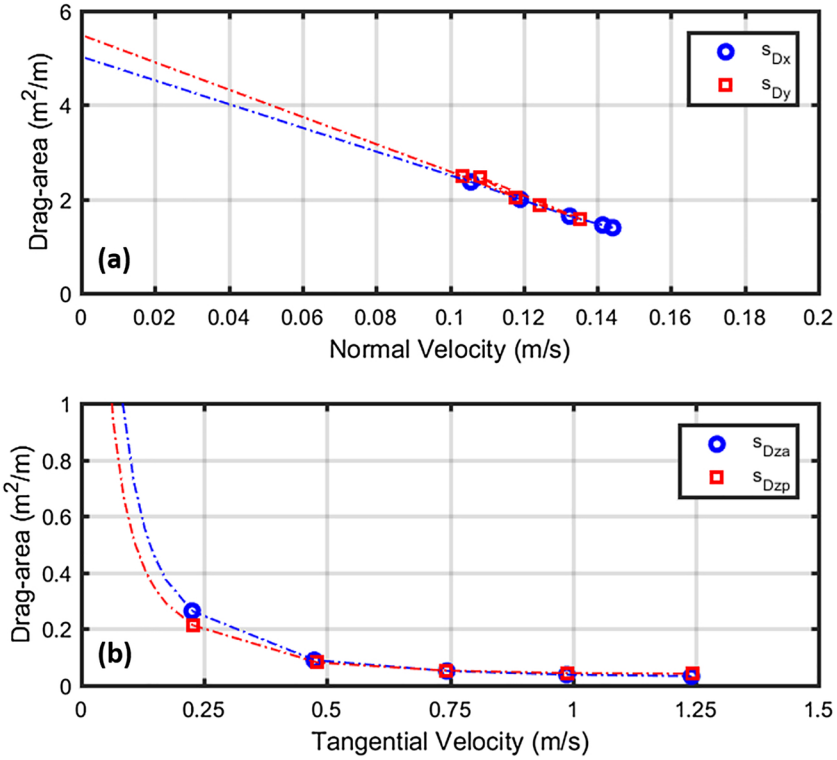

Fig. 12. The extrapolation of normal (a) and tangential (b) drag-area values for speeds between 0 - 0.25 m/s as a function of component velocities.

streamlining effect that enhances kelp survival in energetic, oceanic environments. Evidence of the physical model representing the response of actual kelp is shown in Fig. 13(a) and (b). The visual information first shows a frame shot of tow test video in Fig 13 (a) at the speed setting of 0.25 m/s for the aligned orientation near the reconfiguration threshold. In-situ aggregate observations are shown on

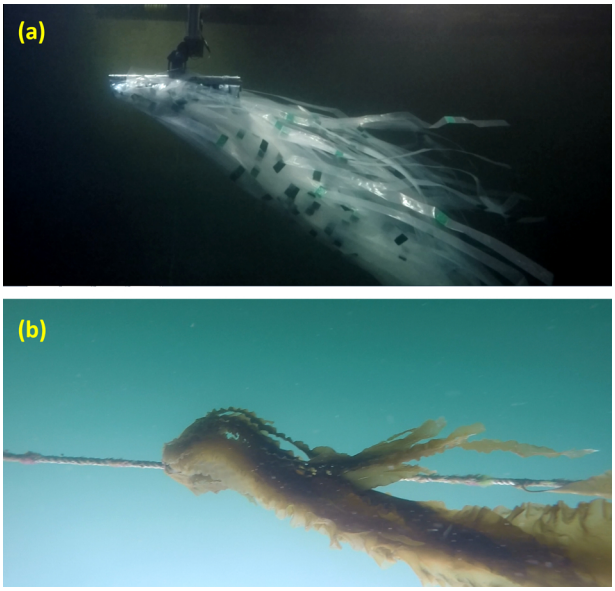

Fig. 13. (a) Video frame shot of the kelp model being towed at 0.25 m/s. (b) Submersible video frame shot of a clump of kelp blades obtained near harvest of the 2017-2018 field season. The kelp line in the Figure has a diameter of 12.7 mm and is made with twisted, 3-strand rope.

Fig 13 (b) made prior to a harvest in May 2018. The field observations shows a clump of blades on a bare section of the kelp line being deflected to a shallower angle. Current velocities at the site are typically on the order of 0.25-0.30 m/s during the middle of the tide, also when the frame shot was acquired. For reference, the kelp line in the Figure has a diameter of 12.7 mm and is made with twisted, 3-strand rope. From these similar response observations, it became clear that both normal and tangential drag forces must be resolved to produce high-fidelity models in dynamic ocean environments with unsteady waves and currents.

4.2. The basis for a numerical modeling approach

By resolving the normal and tangential drag components with the tank test datasets, drag-areas values were calculated that are applicable to unsteady, multidirectional flow. Furthermore, these drag-areas should be applicable for aggregates of aquaculture grown kelp over a wide range of lengths, densities, and environmental conditions. The drag-area values can be incorporated into numerical modeling approaches, of which several exist (Tsukrov et al., 2003; Berstad et al., 2012; Cifuentes and Kim, 2017; Berstad and Heimstad, 2019; Knysh et al., 2020). In these computer models, the normal and tangential drag-area values can be employed with Morison equation forcing (Morison et al., 1950) on dynamic structural components. One option is to develop numerical models with beam entities constructed with finite elements. These beam models can be sufficiently discretized to resolve bending along the kelp aggregate representation. Geometric and material properties for the beam elements of specific kelp morphologies can be obtained from *in-situ* measurements of weight both in and out of water to obtain volume and mass density. Values for EI can also be obtained for actual kelp. Thus, the formulation described in this paper enables a dynamic representation of cultured kelp, a necessary step in the design of optimized kelp aquaculture systems. However, since the Morison equation technique employed in these numerical modeling approaches does not typically calculate wake effects, just simply applying the drag-area results as input does not specifically shed light on the influence of kelp aquaculture systems in the fluid flow field.

5. Conclusions

This study resolved both the normal and tangential drag components acting on a physical model of kelp aggregate using a set of tow tank tests. The full-scale model was built in an effort to match morphological and mechanical properties of densely grown kelp from an aquaculture system in Saco Bay Maine, USA. The model consisted of 178 proxy blades representing a yield of 16.11 kg/m. The forces from the experimental test replicates were processed to obtain normal and tangential drag-area components relative to aggregate angle and speed. The drag-area approach was applied because reference areas for actual kelp aggregates are difficult to quantify and have the potential to take multiple forms in dynamic flow fields of waves and currents propagating from different directions. In steady flows with increasing speed, a point was identified that represents the transition from normal to tangential drag dominance, defining a reconfiguration threshold. This dynamic transition reinforces the need to resolve the drag components relative to the instantaneous velocity vector. Many existing computer modeling techniques employ a multidimensional Morison equation approach to calculate drag forces from relative velocity components. The drag-area values obtained from this study can be applied in these models using Morison equation at sub-meter scales, especially if kelp aggregates are modeled as beam elements. The sub-meter discretization of a beam allows calculation of drag components along a bending finite element to take into consideration aggregate length, EI, volume and mass density, which can be obtained from in-situ values. Implementing this drag calculation in dynamic numerical models will enable more accurate prediction of fluid loads on these systems to further develop the kelp aquaculture industry.

CRediT authorship contribution statement

David W. Fredriksson: Conceptualization, Methodology, Investigation, Validation, Formal analysis, Supervision, Project administration, Funding acquisition, Writing - original draft, Writing - review & editing. **Tobias Dewhurst:** Conceptualization, Methodology, Software, Investigation, Validation, Formal analysis, Writing - review & editing. **Andrew Drach:** Software, Writing - review & editing. **William Beaver:** Resources, Data curation. **Adam T. St. Gelais:** Conceptualization, Resources, Writing - review & editing. **Kathryn Johndrow:** Resources. **Barry A. Costa-Pierce:** Conceptualization, Resources, Project administration, Funding acquisition.

Declaration of Competing Interest

The authors declare that they have no known competing financial interests or personal relationships that could have appeared to influence the work reported in this paper.

Acknowledgements

We would like to express our sincere thanks to the former Midshipmen, S. Riedel, K. Robinson, C. Sowerby, K. Mortenson, L. Haller and S. Toski. With their inspiration and hard work, macroalgae research at the U.S. Naval Academy became possible. Original funding for the field work of this project was obtained from the U.S. National Science Foundation project 13355457 to the Established Program to Stimulate Competitive Research (EPSCoR) of Maine with the University of New England as a partner. The Morton Kelly Foundation also provided initial funding to the University of New England. The U.S. Naval Academy was funded through the ARPA-E Interagency Agreement No. 89703018SAR000002. Additional funding for the University of New England was also through ARPA-E with project No. is DE-AR0000917. The authors would finally like to sincerely thank all of the professional staff at the U.S. Naval Academy, Hydromechanics Laboratory, and the staff of the Marine Science Center at University of New England.

References

Augyte, S., Yarish, C., Redmond, S., Kim, J.K., 2017. Cultivation of a morphological distinct strain of the sugar kelp, Saccharina latissima forma angustissima, from coastal Maine, USA, with implications for ecosystem services. J. Appl. Phycol. 29 (4), 1967–1976. https://doi.org/10.1007/s10811-017-1102-x.

Augyte, S., Lewis, L., Lin, S., Neefus, C.D., Yarish, C., 2018. Speciation in exposed intertidal zone: the case of Saccharina angustissima comb. nov. & stat. nov. (Laminariales, Phaeophyceas). Phycologia 57 (1), 100–112. https://doi.org/10.2216/17-40.1.

Berstad, A.J., Heimstad, L.F., 2019. Analysis of flexible net structures in marine environment. In: Bensow, R., Ringsberg, J. (Eds.), Proceedings of VIII International. Conference on Computational Methods in Marine Engineering MARINE.

Berstad, A.J., Walaunet, J., Heimstad, L.F., 2012. Loads from currents and waves on net structures. In: ASME 2012 31st International Conference on Ocean, Offshore and Arctic Engineering. American Society of Mechanical Engineers. pp. 95–104.

Boller, M.L., Carrington, E., 2006. The hydrodynamic effects of shape and size change during reconfiguration of a flexible macroalga. J. Exp. Biol. 209 (10), 1894–1903. https://doi.org/10.1242/jeb.02225.

Buck, B.H., Buchholz, C.M., 2005. Response of offshore cultivated *Laminaria saccharina* to hydrodynamic forcing in the North Sea. Aqua. 250, 674–691. https://doi.org/10.1016/j.aquaculture.2005.04.062.

Casarella, M.J., Parsons, M., 1970. Cable Systems under hydrodynamic loading. Mar. Technol. Soc. J. 4 (4), 27–44.

Cifuentes, C., Kim, M.H., 2017. Hydrodynamic response of a cage system under waves and currents using a Morison-force model. Ocean Eng. 141, 283–294. https://doi.org/10.1016/j.oceaneng.2017.06.055.

Coleman, H.W., Steele, W.G., 1995. Engineering application of experimental uncertainty Analysis. AIAA Stud. J. 33 (10), 1888–1896. https://doi.org/10.2514/3.12742.

Demes, K.W., Carrington, E., Gosline, J., Martone, P.T., 2011. Variation in anatomical and material properties in hydrodynamic performance of foliose red macroalgae (Rhodophyta). J. Phycol. 47 (6), 1360–1367. https://doi.org/10.1111/j.1529-8817.2011.01066.x.

Faltisen, O.M., 1991. Sea Loads on Ships and Offshore Structures. Cambridge University Press 340 p.

Fredriksson, D.W., Steppe, C.N., Wallendorf, L., Sweeney, S., Kriebel, D.L., 2010. Biological and hydrodynamic design considerations for vertically oriented oyster grow out structures. J. Aquac. Eng. 42, 57–69. https://doi.org/10.1016/j.aquaeng.2009.11.002.

Gaylord, B., Denny, M.W., 1997. Flow and flexibility. I. Effects of size, shape and stiffness in determining wave forces on the stipitate kelps eisenia arborea and pterygophora californica. J. Exp. Biol. 200 (24), 3141–3164.

Goodno, B.J., Gere, J.M., 2020. Mechanics of Materials, 9th edition. Cengage Learning, Inc. 1184 p.

Henry, P.T., 2014. Bending properties of a macroalga: adaptation of Peirce's cantilever test for in-situ measurements of *Laminaria digitate* (*Laminariaceae*). Brief Comm. Amer. J. of Bot. 101 (6), 1050–1055.

Hoerner, S.F., 1965. Fluid-Dynamic Drag. N.J. Published by the Author, Midland Park.

Kim, J.K., Kraemer, G.P., Yarish, C., 2015. Use of sugar kelp aquaculture in Long Island Sound and the Bronx River Estuary for nutrient extraction. Mar. Ecol. Prog. Series. 531, 155–166. https://doi.org/10.3354/meps11331.

Knysh, A., Tsukrov, I., Chambers, M., Swift, M.R., Sullivan, C., Drach, A., 2020. Numerical modeling of submerged mussel longlines with protective sleeves. J. Aquac. Eng. 88. https://doi.org/10.1016/j.aquaeng.2019.102027.

Luhar, M., Nepf, H., 2011. Flow-induced reconfiguration of buoyant and flexible aquatic vegetation. Limnol. Oceanogr. 56 (6), 2003–2017. https://doi.org/10.4319/lo.2011.56.6.2003.

Luhar, M., Nepf, H., 2017. Flow-induced reconfiguration of buoyant and flexible aquatic vegetation. Limnol. Oceanogr. 56 (6), 2003–2017. https://doi.org/10.4319/lo.2011.56.6.2003.

Moffat, R.J., 1988. Describing the uncertainties in experimental results. Exp. Therm. Fluid Sci. 1, 3–17. https://doi.org/10.1016/0894-1777(88)90043-X.

Morison, J.R., Johnson, J.W., O'Brien, M.P., Schaaf, S.A., 1950. The forces exerted by surface waves on piles. Petrol. Trans., Am. Inst. Mining Eng. 149–157. https://doi.org/10.2118/950149-G.

Peirce, F.T., 1930. The "handle" of cloth as a measurable quantity. J. Textile Inst. Trans. 21 (9), T377–T416. https://doi.org/10.1080/19447023008661529.

Rominger, J.T., Nepf, H.M., 2014. Effects of blade flexural rigidity on drag force and mass transfer rates in model blades. Limnol. Oceanogr. 59 (6). https://doi.org/10.4319/lo.2014.59.6.2028. 2028–2014.

Schultz, M.P., 2005. Frictional resistance of antifouling coating systems. ASME. J. Fluids Eng. 126 (6), 1039–1047. https://doi.org/10.1115/1.1845552. November 2004.

Statzner, B., Lamouroux, N., Nikora, V., Sagne, P., 2006. Opinion: the debate about drag and reconfiguration of freshwater macrophytes: comparing results by three recently discussed approaches. Freshw. Rev. 51 (11), 2173–2183. https://doi.org/10.1111/j.1365-2427.2006.01636.x.

Stewart, H.L., 2006. Hydrodynamic consequences of flexural stiffness and buoyancy for seaweeds: a study using physical models. J. Exp. Biol. 209, 2170–2181. https://doi.org/10.1242/jeb.02254.

Tsukrov, I., Eroshkin, O., Fredriksson, D., Swift, M.R., Celikkol, B., 2003. Finite element modeling of net panels using consistent net element. Ocean Eng. 30 (2), 251–270. https://doi.org/10.1016/S0029-8018(02)00021-5.

Vettori, D., Nikora, V., 2017. Morphological and mechanical properties of blades of Saccharina latissima. Estuar. Coast. Shelf Sci. 196, 1–9. https://doi.org/10.1016/j.ecss.2017.06.033.

Vettori, D., Nikora, V., 2018. Flow–seaweed interactions: a Laboratory study using blade models. Environ. Fluid Mech. 18 (3), 611–636. https://doi.org/10.1007/s10652-017-9556-6.

Vettori, D., Nikora, V., 2019. Flow–seaweed interactions of Saccharina latissima at blade scale: turbulence, drag force, and blade dynamics. Aquat. Sci. Mech. 81, 61. https://doi.org/10.1007/s00027-019-0656-x.

Vogel, S., 1984. Drag and flexibility in sessile organisms. Am. Zool. 24 (1), 37–44. https://doi.org/10.1093/icb/24.1.37.